The interaction of surface water waves with submerged breakwaters

M. Christou [a], C. Swan [a,*] O. T. Gudmestad [b]

[a] *Department of Civil & Environmental Engineering, Imperial College London, London SW7 2AZ, UK.*

[b] *Statoil & University of Stavanger, 4035 Stavanger, Stavanger, Norway.*

Abstract

This paper concerns the behaviour of nonlinear regular waves interacting with rectangular submerged breakwaters. A new series of experimental results is presented and compared with numerical calculations based upon a Boundary Element Method (BEM) that utilises multiple fluxes to deal with the discontinuities encountered at the corners of the domain. Specifically, comparisons concern both the spatial water surface profiles at various times and the spatial evolution of the harmonics generated by the breakwaters, the latter being an important focus for the paper. The BEM is shown to accurately model both the water surface profile and the harmonic generation, provided the breakwater width is sufficient to ensure that flow separation is not a controlling influence. Furthermore, evidence is provided to confirm that reflection from rectangular submerged breakwaters is fundamentally a linear phenomenon.

Key words: submerged breakwaters, wave-structure interaction, harmonic generation, multiple-flux boundary element method

1 Introduction

Submerged breakwaters are widely used in coastal regions, often being the preferred solution when full wave protection is not required. They are utilised in a wide variety of tasks, such as protecting harbour entrances, reducing the rate of littoral drift and creating artificial fishing grounds. In practice, submerged breakwaters come in a variety of shapes and their performance is usually assessed on the basis of physical model studies. However, the purpose of the present paper is to demonstrate that some important aspects of the resulting wave-structure interaction, notably the harmonic generation as a surface wave passes over the structure, can be accurately modelled using a fully nonlinear boundary element method. In contrast, other aspects of the interaction are shown to be fundamentally linear and can be successfully modelled using existing analytical procedures irrespective of the steepness of the incident waves. In considering these effects, the paper restricts its attention to breakwaters of rectangular form.

In a coastal engineering context the transmissive property of a breakwater, minimised by reflecting and dissipating the incident wave energy, is of primary importance. However, when $\delta = H/d$ is large and $\mu = kd$ is small (where H is the wave height, d the water depth upstream of the breakwater and k the incident wave number), harmonic generation or decomposition occurs above the breakwater. This phenomenon results in energy being transferred from the first harmonic to higher *bound* (or phase-locked) harmonics of the incident wave (Mei and Ünlüata, 1972). On re-entering deeper water, on the

* Corresponding author. Tel: +44(0)2075945999, Fax: +44(0)2075945991
Email address: c.swan@imperial.ac.uk (C. Swan).

downstream side of the breakwater, these higher harmonics are released as *free* waves. This has a significant impact on the transmitted wave energy, not least because it does not take the form of a monochromatic wave train as predicted by linear theory. With an increase in the steepness of the incident waves, this highly nonlinear phenomenon becomes more significant and, as a result, the existing analytical solutions for wave transmission have proven unsatisfactory.

In part, the motivation for the present study arose from some initial comparisons with the experimental observations of Driscoll et al. (1992); the numerical model of Hague and Swan (2008) providing a better description of the laboratory data than other BEM solutions, notably the model proposed by Grilli et al. (1989). To confirm this result, and to extend the data to include a far wider range of incident wave steepnesses, the present study was undertaken.

This paper continues in §2 with a brief review of the background literature. This leads into a short summary of the BEM model and a description of the experimental study in §3 and §4 respectively. Comparisons between the laboratory observations and the model predictions are provided in §5, with some conclusions and wider implications drawn in §6.

2 Background

Many authors have contributed to the study of submerged breakwaters. In analytical models most theories assume that the reflected and transmitted waves have the same frequency as the incident wave, satisfying a linear scattering problem. Historically, Lamb (1932) derived expressions for the reflection, K_r, and transmission, K_t, coefficients due to an infinite step; the solutions based

upon the assumptions that the incident wavelength, λ, is large in comparison to both the upstream water depth, d, and the depth of submergence of the crest of the breakwater, d_s. Dean (1945) developed a linear theory to calculate K_r and K_t for thin breakwaters in infinitely deep water; Ogilvie (1960) provided the equivalent shallow water solutions; whilst Takano (1960) developed a linear theory that was applicable for all relative water depths and crest widths (B/λ, see notation defined on Fig. 1).

On the topic of harmonic generation, Mei and Ünlüata (1972) investigated wave propagation in shallow water of constant depth, in the absence of any breakwater. They observed significant transfers of energy to the higher harmonics for $kd < 0.6$, and attributed these transfers to resonant interactions between the first and second harmonics. Massel (1983) developed a second-order theory for both finite and infinite steps by linearly decomposing the second-order scattered potential, using the wave steepness, $Hk/2$, as the perturbation parameter. Comparisons between these results and experimental data showed that whilst the second harmonic was reasonably well predicted, the modulation of the first harmonic over high steps ($d_s/d = 0.47$) was not.

Dattatri et al. (1978) performed a wide ranging laboratory study of submerged breakwaters and found the most influential parameters affecting K_t were the relative crest width, B/λ, and the relative depth of submergence, d_s/d (Fig. 1). More recently, Rey et al. (1992) presented experimental studies of K_r and the harmonic generation produced by monochromatic linear waves ($0.002 \leqslant Hk/2 \leqslant 0.06$) interacting with solid rectangular steps composed of both sharp and rounded corners. They compared their measurements to the linear theories of Takano (1960) and Devillard et al. (1988) showing that both analytical models accurately predicted K_r, but gave differing results for

the harmonic generation. Rey et al. (1992) also undertook flow visualisation studies to investigate the influence of the incident amplitude and the curvature of the corners and, as expected, found that the higher the incident wave amplitude and the sharper the corners the greater the flow separation.

Numerically, shallow water phenomena are commonly described using Boussinesq models, examples including Battjes and Beji (1992) and Eldeberky and Battjes (1994). However, several authors have also tackled the problem using a boundary element approach. For example, Ohyama and Nadaoka (1992) used a BEM to investigate the harmonic generation resulting from the interaction of regular and irregular waves with finite and infinite steps. They concluded that the transfer of energy to the higher harmonics was critically dependent on the ratio between the crest width of the breakwater and the beat length of the relevant harmonic; the latter being discussed in §5.2.

Driscoll et al. (1992) undertook a similar study to the present one; comparing experimental results with the fully nonlinear BEM method of Grilli et al. (1989) for rectangular impermeable submerged obstacles. Specifically, they investigated the harmonic generation produced by a linear incident regular wave of steepness $Hk/2 = 0.019$ interacting with a rectangular obstacle of vertical aspect ratio $d_s/d = 0.24$. In addition, Driscoll et al. (1992) measured the reflection and transmission coefficients for a variety of wave steepnesses and compared them to the linear scattering model of Losada (1991). These results showed that the linear model accurately predicted the reflection coefficient, but overestimated the transmission coefficient. In explaining these results Driscoll et al. (1992) concluded that this discrepancy was caused by a combination of dissipation, due to frictional and turbulent loses, and the energy transfer to higher harmonics. These conclusions are in broad agree-

ment with the earlier work of Dick and Brebner (1968) who claimed (for the cases that they investigated) between 36% to 64% of the transmitted wave energy is transferred to higher harmonics of the incident wave. It is clear from these results alone that if wave transmission over a submerged breakwater is to be effectively modelled, an appropriate theory or model must incorporate nonlinear harmonic generation.

The present paper adds to this discussion in two respects. First, it provides laboratory observations concerning nonlinear incident regular waves. In terms of the wave steepness, $Hk/2$, the present wave conditions are 2.5 and 10 times steeper than those of Beji et al. (1992) and Driscoll et al. (1992) respectively. Second, comparisons with a multiple-flux BEM model will demonstrate that these important effects can be reproduced by fully nonlinear computations. Although these contributions are significant, it is nonetheless important to note that the BEM provides a potential flow solution and cannot therefore incorporate the effects of wave breaking, particularly the associated energy dissipation. Whilst this is undoubtedly an important limitation, Gu and Wang (1992) note that on the basis of experimental observation the transmission coefficient, K_t, hardly varies once the breaking limit is exceeded. Furthermore, Battjes and Beji (1992) showed that breaking does not significantly affect the energy transfers associated with harmonic generation; the energy being dissipated from all frequencies in an average sense.

3 Boundary Element Method (BEM)

Longuet-Higgins and Cokelet (1976) were the first to apply the Boundary Integral Equation (BIE) to the description of surface water waves. Building upon

this important lead, several authors have made significant contributions; the models associated with the latter being broadly divided into two categories. The first involves models based upon the Cauchy integral formula. This is a conformal mapping scheme that has been very successfully applied in two-dimensions by Dold and Peregrine (1984). Although this has been shown to be accurate and efficient, it involves calculations in the complex plane, and cannot, therefore, be extended to three-dimensions. In contrast, more recent efforts (Grilli et al., 1989) have focused on using Green's second identity. This is located in physical space, can be applied to three-dimensional simulations, and is not constrained by periodicity or uniform depth (Grilli et al., 2001). Within this second category, Hague and Swan (2008) have developed a physical space BEM that utilises multiple fluxes to overcome the corner problem (discussed in §3.3) and describe surface water waves without smoothing, filtering or re-griding of any kind. This is particularly important in problems involving significant energy shifts, the magnitude of which cannot be determined *a priori*. In earlier studies, this model has accurately simulated several realistic three-dimensional JONSWAP sea-states with vast numbers of frequency and directional components (Hague and Swan, 2006). In the present study the two-dimensional formulation of this model (Hague and Swan, 2008) has been extended to include structures within the computational domain. This introduces more corners or geometric discontinuities, but in this case they define the principal area of interest (the submerged breakwater) rather than merely being located on the periphery of the domain as is the case in a standard numerical wave tank. Clearly this provides a stringent test of the performance of the multiple flux approach.

3.1 Governing Equations

With the fluid assumed to be incompressible and inviscid and the flow irrotational, mass continuity is defined by Laplace's equation and must be satisfied throughout the fluid domain such that

$$\nabla\phi^{\,2} = 0, \tag{1}$$

where $\phi(x, z, t)$ is the velocity potential. In the spatial domain a fundamental solution to (1) is given by Green's function, $G(p, q) = -\frac{1}{2\pi}\ln(r(p, q))$, where $r(p, q) = |\mathbf{x}_p - \mathbf{x}_q|$ with $\mathbf{x}_p$ and $\mathbf{x}_q$ the source and evaluation points on the boundary respectively. Applying Green's second identity, the dimensionality is reduced by one and the Boundary Integral Equation (BIE) results

$$C(p)\phi(p) + \int_\Gamma \phi(q)\frac{\partial G(p, q)}{\partial n}\,\mathrm{d}\Gamma(q) = \int_\Gamma G(p, q)\frac{\partial \phi(q)}{\partial n}\,\mathrm{d}\Gamma(q), \tag{2}$$

where $\mathbf{n}$ is the unit outward normal, Γ defines the boundary of the domain, and $C(p)$ is a function of the position of the source on the boundary; the latter calculated using a rigid mode technique (Becker, 1992).

3.2 Boundary Conditions

The model utilises mixed boundary conditions, consisting of *Neumann* conditions (prescribed $\partial\phi/\partial n$) on the bed, left and right boundaries (Γ_b, Γ_l and Γ_r respectively) and a *Dirichlet* boundary condition (prescribed ϕ) on the water surface (Γ_s). Further details of the computational domain and the notation

employed are given in Fig. 1 and Fig. 2.

Taking each of the boundaries in turn:

(a) The left boundary, Γ_l, is defined as a *semi-Lagrangian input* boundary on which the Stokes' fifth analytical velocities corresponding to a regular wave train are prescribed following the solution of Fenton (1985). Along this boundary the nodes are free to move vertically, but not horizontally.

(b) On the bed, Γ_b, which includes the impermeable submerged breakwater, a zero flux condition is imposed, $\frac{\partial \phi}{\partial n} = 0$.

(c) On the right boundary, Γ_r, a Sommerfeld (1949) radiation condition is applied

$$\frac{\partial \phi}{\partial x} = -\frac{1}{c} \left. \frac{\partial \phi}{\partial t} \right|_{x_{up}, t-\Delta t}, \tag{3}$$

where c is the known phase velocity corresponding to the input waves, $x_{up} = x - c\Delta t$ with x being the horizontal coordinate of the right-hand side nodes and Δt the time step. Equation (3) is applied at the corner node, at the intersection between the water surface and the right boundary. For the remainder of the nodes on Γ_r, a linear velocity profile scaled to match the horizontal velocity at the water surface, equation (3), is applied to approximate the radiation condition with depth below the water surface. Hague (2006) showed that for a regular wave, this radiation condition results in a reflection coefficient that is less than 2%.

(d) Finally, on the water surface, Γ_s, a velocity potential of $\phi = 0$ is initially prescribed to model still water.

3.3 Multiple Fluxes

With the boundary element approach derived in physical space, the corners of the domain create certain difficulties. Indeed, they represent geometric discontinuities and with the BIE (2) requiring a smooth boundary, these discontinuities give rise to the so-called *corner problem*. Traditionally, BEM-based wave models have overcome this hurdle using the double-node approach (Grilli and Svendsen, 1990). In contrast, Hague and Swan (2008) introduced the multiple flux technique of Brebbia and Dominguez (1992) to numerical wave simulations. This method specifies only one node at a corner, but considers all of the fluxes associated with that location. With the introduction of a submerged breakwater, several additional geometric discontinuities are introduced. An accurate treatment of the corner problem is essential, not least because these additional corners lie central to the domain. Indeed, they define an essential part of the problem to be solved; the submerged breakwater. The numerical model of Hague and Swan (2008) is used throughout this paper and its successful treatment of the corners is believed to be fundamental to the success of the calculations.

3.4 System of Equations

In order to evaluate the BIE (2), the boundary of the fluid domain is discretised into M isoparametric quadratic elements, resulting in N nodes (Becker, 1992). The discretised version of the BIE is numerically integrated by Gaussian quadrature, resulting in a linear system of equations

$$\mathbf{H}\left\{\phi\right\} = \mathbf{G}\left\{\frac{\partial\phi}{\partial n}\right\}, \tag{4}$$

where $\mathbf{H}$ (size $N \times N$) and $\mathbf{G}$ (size $N \times 3M$, as there are now three fluxes per element due to the multiple flux technique) are coefficient matrices and $\{\phi\}$ (size $N \times 1$) and $\{\partial\phi/\partial n\}$ (size $3M \times 1$) are the column vectors of all the ϕ and $\partial\phi/\partial n$ variables respectively. After applying the mixed boundary conditions, the unknown values are transferred to the left-hand side by swapping the elements of the vectors $\{\phi\}$ and $\{\partial\phi/\partial n\}$ resulting in a linear system of equations

$$\mathbf{A}\mathbf{x} = \mathbf{b}, \tag{5}$$

where $\mathbf{A}$ is the influence matrix, $\mathbf{x}$ contains all the unknown variables and $\mathbf{b}$ is the vector determined by the matrix-vector product of the known quantities. The unknown vector, $\mathbf{x}$, is then determined using the GMRES iterative solver (Saad and Schultz, 1986) with a Jacobi preconditioner (Barrett et al., 1994; Trefethen and Bau III, 1997), reducing the computational effort from $O(N^3)$ to $O(N^2)$.

3.5 Free Surface and Time Marching

A semi-Lagrangian framework is used throughout the present simulations, allowing the nodes to move vertically but not horizontally. The free surface is defined by both the Kinematic Free Surface Boundary Condition (KFSBC)

$$\frac{\delta\eta}{\delta t} = \frac{\partial\phi}{\partial z} - \frac{\partial\phi}{\partial x}\,\frac{\partial\eta}{\partial x}\,, \tag{6}$$

and the Dynamic Free Surface Boundary Condition (DFSBC)

$$\frac{\delta\phi}{\delta t} = -g\eta - \frac{1}{2}\left[\left(\frac{\partial\phi}{\partial x}\right)^2 + \left(\frac{\partial\phi}{\partial z}\right)^2\right] + \frac{\partial\phi}{\partial z}\left(\frac{\partial\phi}{\partial z} - \frac{\partial\phi}{\partial x}\,\frac{\partial\eta}{\partial x}\right), \tag{7}$$

where $\delta/\delta t$ denotes a time derivative in the semi-Lagrangian frame. With the right-hand side of both (6) and (7) independent of time, they can be treated

as ordinary differential equations and time marched to obtain values of η and ϕ at the next time step. This mixed Eulerian-Lagrangian time marching is undertaken using the fourth-order predictor-corrector method of Adams-Bashforth-Moulton. As this method requires information from three previous time steps, it is necessary to kick-start the model by using three steps of a fourth-order Runge-Kutta integration scheme; the latter being a single step method.

4 Experimental Investigations

The experiments were performed in a glass-walled wave flume located in the Hydrodynamics Laboratory in the Department of Civil & Environmental Engineering at Imperial College London. The flume is equipped with bottom-hinged, flap-type, wave makers located at either end. These are capable of generating and absorbing unidirectional waves in the frequency range $0.3\text{Hz} \leqslant f \leqslant 3\text{Hz}$. The flume is 27m long, 0.3m wide and has an operating water depth of $d = 0.7\text{m}$.

The study considered four submerged breakwaters, each subject to three different regular wave conditions. All of the breakwaters were rectangular extending the full width of the flume with a height of $h = 0.35\text{m}$; the latter representing a relative depth of submergence of $d_s/d = 0.5$. The four breakwaters correspond to crest widths of $B = 1.5\text{cm}$, 35cm, 70cm and 105cm; the front of each being located 13.35m from the generating paddle. A sketch showing the layout of the experimental apparatus is given on Fig. 3.

The three regular wave conditions were selected to cover a broad range of

steepness and hence nonlinearity. The wave period was held constant at $T = 1.28$s, resulting in $kd = 1.94$ on the upstream and downstream sides of the breakwater, and $kd_s = 0.97$ above the structure, with a corresponding incident wave number of $k = 2.77\,\mathrm{rad/m}$. With the wave heights for the three cases corresponding to $H = 39.2$mm, 106.2mm and 142.1mm, the wave steepness is $Hk/2 = 0.054$, 0.147 and 0.197 representing linear, weakly nonlinear and nonlinear incident waves respectively. Full details of the wave parameters adopted in the present study are given in Table 1. In line with earlier discussions, the nonlinear case was chosen to be as steep as possible, whilst avoiding the occurrence of wave breaking during its interaction with the breakwater having the largest crest width ($B = 105$cm). With the absence of wave breaking, comparisons to the BEM were possible over the full range of test conditions.

Within the laboratory study the water surface elevations were recorded using surface-piercing, resistance, wave gauges. Each gauge provides a time-history of the water surface elevation, $\eta(t)$, at one location fixed in space; earlier studies having shown that such measurements can be achieved with an accuracy of ± 0.5mm with no significant disturbance of the wave field. In each test a control gauge was located 2.85m from the generating wave paddle, allowing the repeatability of the waves to be monitored. An array of twenty gauges, with individual wave gauges equally spaced at 20mm apart, was used to measure $\eta(t)$ in the immediate vicinity of the breakwater. By moving the array into five different locations, and repeating the measurements, data were recorded from 20mm upstream to 1.32m downstream of the front of the breakwater. In all cases some overlap between the gauge locations provided a second check of the repeatability of the generated waves. In each test case, the wave conditions were first run without any structure present (on a flat bed) and then re-run

with each of the four breakwaters in turn; the difference between these records identifying directly the disturbance or change caused by the presence of the submerged breakwater.

5 Discussion of Results

The computational domain used for the numerical runs was identical to the experimental set-up given in Fig. 3; the only exception being that the generating and absorbing wave paddles are replaced with the *semi-Lagrangian input* and the radiation condition respectively, both described in §3.2. The number of elements employed to discretise the computational domains and the typical run times per step are given in Table 2. Furthermore, the time histories of the water surface elevation, $\eta(t)$, were obtained from the BEM via numerical wave gauges located at the same positions as their experimental counterparts.

To ensure a valid comparison between the experimental and numerical data describing the wave-structure interaction, the incident wave conditions must be identical. Fig. 4 concerns the time-history of the water surface elevation, for each of the three wave cases, measured in the absence of a structure (on a flat bed). The data relate to conditions 13.95m from the generating paddle and demonstrates excellent agreement between the measured and predicted incident waves.

Although the absorbing wave paddle, located at the downstream end of the wave flume, efficiently dissipated most of the incident wave energy, small unwanted reflections from this downstream boundary will eventually contaminate the measured data. To avoid this the sample time was chosen to lie

between the arrival of the steady regular waves and the instant at which reflections from the absorbing paddle arrive back at the measuring section. This corresponded to a time interval of 24s $\leqslant t \leqslant$ 32s, where $t = 0$s coincides with the onset of wave generation. All the data presented below were sampled within this range and must therefore be independent of any small spurious effects arising at the downstream boundary.

5.1 Spatial Water Surface Profiles

Figs. 5, 6, 7 and 8 concern spatial water surface profiles in the vicinity of the submerged breakwaters, providing comparisons between the laboratory data and the BEM model predictions for the four crest widths of $B = 1.5$cm, 35cm, 70cm and 105cm respectively. In each case, comparisons are provided for four different times, corresponding to different phases of the wave cycle, and for all three incident wave cases. In addition, spatial profiles calculated without the structures present are also plotted to indicate the influence of the submerged breakwaters on the water surface. In each of these figures it is clear that the BEM model compares very favourably with the experimental observations.

Given the relative submergence of $d_s/d = 0.5$, it is to be expected that the breakwater with the smallest crest width ($B = 1.5$cm on Fig. 5) has a negligible influence on the surface profile. However, with increasing crest width, the influence of the submerged structure becomes clear: the steepening of the wave profile and the decrease in the phase velocity being clearly noted, particularly in Figs. 6(f), 7(f) and 8(f). In comparing these cases the decrease in the phase velocity is of the order of 15%. This latter value does not appear to be strongly dependent upon the incident wave steepness, and is surprisingly

consistent for the largest three breakwaters ($B = 35$cm, 70cm and 105cm). In contrast, the wave steepness continues to increase with the breakwater crest width. This, in turn, indicates that the shallower water over the structure introduces significant nonlinearity. Indeed, Eldeberky and Battjes (1994) state that this increased nonlinearity in the shallower region, above the submerged breakwater, amplifies the *bound* harmonics. These are then released as *free* waves downstream of the breakwater where the water depth once again increases and the nonlinearity must necessarily reduce.

5.2 Harmonic Generation

In order to calculate the harmonic generation produced by each of the four breakwater cases, a Fast Fourier Transform (FFT) of the water surface elevation, $\eta(t)$, was used to define the amplitude spectrum at each wave gauge location. Having isolated each harmonic, the spatial evolution of the harmonic amplitudes can be deduced and this is presented in Figs. 9, 10, 11 and 12 corresponding to breakwater crest widths of $B = 1.5$cm, 35cm, 70cm and 105cm respectively. Each figure describes the spatial evolution of the first four harmonic amplitudes present in the experimental observation and in the BEM model predictions; with data provided for each of the three wave cases. For comparative purposes a similar analysis is also undertaken for the incident waves (no structure present), again predicted by the BEM model. In order to facilitate comparisons between the three wave cases, the vertical axes of the linear and weakly nonlinear cases are chosen so that the difference between the maximum and minimum values is identical to that of the corresponding nonlinear case.

With the exception of the results relating to the narrowest breakwater ($B =$ 1.5cm on Fig. 9), the BEM predictions are in good agreement with the experimental observations. The poor BEM predictions in the first case ($B = 1.5$cm) are due to the relative importance of flow separation; the lengths of the shed vortices being large relative to the breakwater width, B. From visual observations the diameter of the shed vortex, D_v, was found to be approximately 1.5cm, 3cm and 4cm for the linear, weakly nonlinear and nonlinear wave cases respectively. Relative to the breakwater crest width $B = 1.5$cm, this corresponds to ratios of $D_v/B = 1.0$, 2.0 and 2.7 for the three wave cases. Comparatively, the ratios for the next widest breakwater, $B = 35$cm on Fig. 10, are significantly smaller at $D_v/B = 0.04$, 0.09 and 0.11. The practical consequences of this is that, as far as the overlying waves are concerned, the shedding of vortices significantly increases the effective crest width of the narrowest breakwater. Furthermore, vortices are shed both upstream and downstream of the structure; the former caused by the negative velocities occurring beneath a wave trough and the latter the positive velocities beneath a wave crest. This results in a moving obstacle, the effective size of which is larger than the physical breakwater. The BEM model is based upon an inviscid irrotational formulation and so does not model flow separation. Hence, the numerical wave field is only influenced by the stationary, narrower breakwater. This accounts for the large discrepancies arising in Fig. 9.

In all the remaining breakwater cases, the trends of the harmonic generation are very well described, with reasonable agreement in the absolute magnitude of the terms involved. Typically, the agreement between the measured and predicted results improves as the breakwater crest width increases and the steepness of the incident wave reduces; the latter implying reduced wa-

ter particle kinematics. This is to be expected and again reflects the relative importance of flow separation and vortex shedding.

It is also important to note that the good description of the harmonic generation holds equally well for the third and fourth harmonics as for the first and second harmonics. In part, this arises because of the lack of smoothing or filtering undertaken in the current BEM formulation and, more generally, reflects the success of the multiple flux approach. Indeed, if we contrast the present comparisons with those made between the experiments of Driscoll et al. (1992) and the BEM of Grilli et al. (1989), the most striking difference lies in the accuracy of the higher harmonic predictions.

With good agreement between the BEM predictions and the experimental observations in the vicinity of the breakwater, it is possible to take advantage of the full spatial information (covering the entire domain) generated by the numerical model. Figs. 13, 14 and 15 concern the spatial evolution of the amplitude of the first three harmonics in the linear and nonlinear wave cases for submerged breakwaters with crest widths of $B = 35$cm, 70cm and 105cm respectively.

Figs. 13(a)(b), 14(a)(b) and 15(a)(b) concern the amplitude of the first harmonic. Upstream of the breakwater ($x \leqslant 13.35$m) there is a marked contrast between the constant amplitude describing the incident waves in the absence of the breakwater and the fluctuating amplitude predicted with the breakwater present; the latter defining the partial standing wave that forms due to the constructive and destructive interference between the incident and reflected waves. In contrast, the second and third harmonic amplitudes (Figs. 13(c)–(f), 14(c)–(f) and 15(c)–(f)) within this same upstream region show no signif-

icant variation between the data generated with and without the breakwater in place. This suggests that wave reflection from a submerged breakwater is dominated by the first harmonic motion. This, in turn, explains the accurate prediction of the reflection coefficient, K_r, by linear theory reported by several authors including Driscoll et al. (1992) and Rey et al. (1992).

Downstream of the breakwater ($x \geqslant 14.4$m) the data presented on Figs. 13, 14 and 15 highlight the importance of the nonlinearity of the incident waves and the subsequent wave interactions in respect of wave transmission and, particularly, the nature of the harmonic generation. For example, comparisons between the linear and nonlinear wave cases identify significant differences in the amplitudes of the harmonics; the effect being particularly marked in respect of the first harmonic. In the linear wave case (Figs. 13(a), 14(a) and 15(a)) the amplitude of the first harmonic remains constant and approximately equal to its value in the incident waves measured in the absence of the breakwater. In contrast, in the nonlinear wave case the amplitude of the first harmonic exhibits significant modulation relative to the data recorded with no structure present. Furthermore, in both the linear and nonlinear wave cases, Figs. 13, 14 and 15 describe a marked increase in the amplitude of the second and third harmonics relative to the incident wave conditions; the amplitudes of these harmonics fluctuating with distance downstream of the breakwater. This latter effect arises because of the interaction (constructive and destructive interference) between the *free* and *bound* waves arising at each harmonic; the two components having different wave numbers and hence different phase velocities.

The first and second harmonic interactions were first described in a second-order theory proposed by Massel (1983). The present results are in broad

agreement with this theory. However, with the BEM calculations retaining the fully nonlinearity of the problem, there are also some important differences. Based upon second-order wave interactions, Massel (1983) defined the spatial variation or beat length of the first and second harmonics as

$$L_t = \frac{2\pi}{k^{(2)} - 2k^{(1)}} \ , \tag{8}$$

where $k^{(1)}$ and $k^{(2)}$ are the wave numbers of the first and second *free* harmonics respectively, with $k^{(2)} \geqslant k^{(1)}$. Within the present study, the constant incident wave period ($T = 1.23$s) defines $L_t = 1.23$m for all cases. Using the results of the BEM calculations, the beat lengths for each of the first three harmonics are presented on Table 3. In the linear wave case, the beat length of the second harmonic ($L_t^{(2)}$) is in very good agreement with that predicted by Massel (1983). However, with an increase in the incident wave steepness the weakly nonlinear and nonlinear wave cases produce beat lengths that are approximately 11% and 23% greater than the value predicted by equation (8).

The data presented in Table 3 also show that for each incident wave steepness, the beat lengths associated with each of the first three harmonics are remarkably similar. An explanation for this lies in the nature of the harmonic generation (Massel, 1983) and the form of the wave interactions (Longuet-Higgins and Stewart, 1960); the combination of the two providing evidence as to which interactions become dominant. When regular waves propagate over a submerged breakwater, the amplitudes of the *bound* higher harmonic waves increase, contributing to the wave steepening observed in Figs. 6, 7 and 8. When the waves propagate off the breakwaters, some proportion of these higher harmonic waves are shed as freely propagating waves; hence the notion of harmonic generation. The downstream wave field therefore consists

of a freely propagating first harmonic ($\omega^{(1)}$, $k^{(1)}$), its associated *bound* harmonics, ($2\omega^{(1)}$, $2k^{(1)}$), ($3\omega^{(1)}$, $3k^{(1)}$) etc., and the newly generated *free* waves ($\omega^{(2)}$, $k^{(2)}$),($\omega^{(3)}$, $k^{(3)}$) etc.; the accompanying notation describing the (wave frequency, wave number) and the superscript denoting the harmonic concerned such that $\omega^{(2)} = 2\omega^{(1)}$ and $\omega^{(3)} = 3\omega^{(1)}$.

In describing the first harmonic, the amplitude fluctuation is due to the interaction between the freely propagating wave ($\omega^{(1)}$, $k^{(1)}$) and a *bound* first harmonic; the latter representing the frequency difference terms arising from the interaction of the first and second harmonic *free* waves ($\omega^{(2)} - \omega^{(1)}$, $k^{(2)} - k^{(1)}$). Having defined the waves involved, the beat length, L_t, is given by $2\pi/\Delta k$, where Δk is the difference in the wave numbers of the interacting waves. In the case of the first harmonic, $\Delta k = (k^{(2)} - k^{(1)}) - k^{(1)}$ and hence $L_t^{(1)}$ is defined by equation (8). In addressing the second harmonic, the key interactions concern the freely propagating second harmonic ($\omega^{(2)}$, $k^{(2)}$) and the *bound* second harmonic resulting from the self-interaction (or Stokes term) involving what is essentially a frequency sum term ($\omega^{(1)} + \omega^{(1)}$, $k^{(1)} + k^{(1)}$). In this case the relevant $\Delta k = k^{(2)} - 2k^{(1)}$ and the beat length $L_t^{(2)}$ is again defined by equation (8). In considering the third harmonic, the problem becomes more complicated because of the number of possible interactions. However, having considered the size of the terms involved and the data presented on Table 3, it appears that the dominant interaction involves two *bound* waves travelling at different velocities. The first of these is the third harmonic Stokes wave ($3\omega^{(1)}$, $3k^{(1)}$) and the second is a frequency-sum term arising from the interaction of the first and second harmonic *free* waves ($\omega^{(1)} + \omega^{(2)}$, $k^{(1)} + k^{(2)}$). In this case $\Delta k = (k^{(1)} + k^{(2)}) - 3k^{(1)}$ with $L_t^{(3)}$ again defined by equation (8).

In seeking to describe the origins of the amplitude modulations, it is inter-

esting to note that whilst the first harmonic involves the interactions with a frequency difference term, the second and third harmonics involve interactions with frequency sum terms. Since *sum* and *difference* terms are typically out of phase, the amplitude modulation of the first harmonic should be 180° out of phase with the amplitude modulation of the second and third. The data presented in Figs. 13, 14 and 15 describes exactly this trend; the relative phasing of the amplitude modulations being completely independent of the breakwater width, B.

6 Conclusions

The present study has considered the propagation of regular waves of varying steepness over submerged rectangular breakwaters of varying crest width and has provided comparisons between laboratory observations and fully nonlinear numerical calculations based upon a multiple-flux boundary element method. These comparisons demonstrate that with an effective treatment of the corner problem, based on the concept of multiple fluxes, very good agreement with the laboratory observations can be achieved. Most importantly, there is no need for smoothing, filtering or re-gridding and there is no ambiguity concerning the generation of higher harmonic wave components downstream of the breakwater.

For the cases considered both the experimental observations and the numerical calculations confirm that the reflection of waves from a submerged breakwater is fundamentally linear, even if the incident waves are nonlinear. This result is consistent with earlier work in which laboratory observations were shown to be in good agreement with reflection calculations based on linear theory;

suggesting that the latter is appropriate to engineering calculations.

In contrast, the wave profile evolving over the breakwaters undergoes significant steepening and nonlinear amplification, with the maximum crest elevation increased by as much as 25%. Likewise, the transmission of waves from the downstream side of the breakwaters is also highly nonlinear, both in terms of the generation of freely propagating wave harmonics and the interaction between the *free* and *bound* wave components; the latter leading to significant amplitude modulation affecting all the harmonic components. Comparisons between these results and the second-order model of Massel (1983) confirm that his estimate of the beat length, or the spatial scale of the amplitude modulation, is broadly correct but subject to large variations depending on the nonlinearity of the wave field. In contrast to the observed reflections, both the evolution of the wave profile over the breakwater and the transmission of waves downstream of the breakwater are highly nonlinear processes and should be modelled accordingly.

Acknowledgements

The authors gratefully acknowledge the financial support provided by the UK Engineering and Physical Sciences Research Council (EPSRC) and Statoil, Norway.

References

Barrett, R., Berry, M., Chan, T. F., Demmel, J., Donato, J. M., Dongarra, J., Eijkout, V., Pozo, R., Romine, C., Vorst van der, H., 1994. Templates

for the Solution of Linear Systems: Building Blocks for Iterative Methods. SIAM, Philadelphia.

Battjes, J. A., Beji, S., 1992. Breaking waves propagating over a shoal. In: Proceedings of 23rd Coastal Engineering Conference, ASCE. pp. 42–50.

Becker, A. A., 1992. The Boundary Element Method in Engineering: A Complete Course. McGraw-Hill Book Company, London.

Beji, S., Ohyama, T., Battjes, J. A., Nadaoka, K., 1992. Transformation of nonbreaking waves over a bar. In: Proceedings of 23rd Coastal Engineering Conference, ASCE. pp. 51–61.

Brebbia, C. A., Dominguez, J., 1992. Boundary Elements: An Introductory Course., 2nd Edition. Computational Mechanics Publications (McGraw-Hill), London.

Dattatri, J., Raman, H., Shankar, N. J., 1978. Performance characteristics of submerged breakwaters. In: Proceedings of the 16th Coastal Engineering Conference, ASCE. pp. 2153–2171.

Dean, W. R., 1945. On the reflection of surface waves by a submerged plane barrier. Proceedings of the Cambridge Philosophical Society 41, 231–238.

Devillard, P., Dunlop, F., Souillard, B., 1988. Localization of gravity waves on a channel with random bottom. Journal of Fluid Mechanics 186, 521–538.

Dick, T. M., Brebner, A., 1968. Solid and permeable submerged breakwaters. In: Proceedings of the 11th Coastal Engineering Conference, ASCE. pp. 1141–1158.

Dold, J. W., Peregrine, D. H., 1984. Steep unsteady water waves: An efficient computational scheme. In: Proceedings of the 19th Coastal Engineering Conference, ASCE. pp. 955–967.

Driscoll, A. M., Dalrymple, R. A., Grilli, A. T., 1992. Harmonic generation and transmission past a submerged obstacle. In: Proceedings of 23rd Coastal

Engineering Conference, ASCE. pp. 1142–1152.

Eldeberky, Y., Battjes, J. A., 1994. Nonlinear coupling in waves propagating over a bar. In: Proceedings of the 24th Coastal Engineering Conference, ASCE. pp. 157–167.

Fenton, J. D., 1985. A fifth-order Stokes theory for steady waves. Journal of Waterway, Port, Coastal and Ocean Engineering 111, 216–234.

Grilli, S. T., Guyenne, P., Dias, F., 2001. A fully non-linear model for three-dimensional overturning waves over an arbitrary bottom. International Journal for Numerical Methods in Fluids 35, 829–867.

Grilli, S. T., Skourup, J., Svendsen, I. A., 1989. An efficient boundary element method for nonlinear water waves. Engineering Analysis with Boundary Elements 6, 97–107.

Grilli, S. T., Svendsen, I. A., 1990. Corner problems and global accuracy in the boundary element solution of nonlinear wave flows. Engineering Analysis with Boundary Elements 7 (4), 178–195.

Gu, G. Z., Wang, H., 1992. Numerical modeling for wave energy dissipation within porous submerged breakwaters of irregular cross section. In: Proceedings of the 23rd Coastal Engineering Conference, ASCE.

Hague, C. H., 2006. Fully nonlinear computations of directional waves, including wave breaking. Ph.D. thesis, Imperial College London.

Hague, C. H., Swan, C., 2006. A boundary element solution applied to the description of extreme waves in coastal waters. In: Proceedings of the 30th Coastal Engineering Conference, ASCE.

Hague, C. H., Swan, C., 2008. On the advantages of a multiple flux boundary element method applied to the description of surface water waves. Submitted to the Journal of Computational Physics.

Lamb, H., 1932. Hydrodynamics. Cambridge University Press.

Longuet-Higgins, M. S., Cokelet, E. D., 1976. The deformation of steep surface water waves on water. A numerical method of computation. Proceedings of the Royal Society London A 350, 1–26.

Longuet-Higgins, M. S., Stewart, R. W., 1960. Changes in the form of short gravity waves. Journal of Fluid Mechanics 8, 565–583.

Losada, I., 1991. Estudio de la propagacion de un tren lineal de ondas por un medio discontinuo. Ph.D. thesis, University of Cantabria, Santander, Spain.

Massel, S. R., 1983. Harmonic generation by waves propagating over a submerged step. Coastal Engineering 7, 357–380.

Mei, C. C., Ünlüata, U., 1972. Harmonic generation in shallow water waves. In: Meyer, R. E. (Ed.), Waves on beaches and resulting sediment transport. Academic Press, pp. 181–202.

Ogilvie, T. F., 1960. Propagation of waves over an obstacle in water of finite depth. Universtiy of California, Institute of Engineering Research Report 82-14.

Ohyama, T. O., Nadaoka, K., 1992. Modeling the transformation of nonlinear waves pasing over a submerged dike. In: Proceedings of the 23rd Coastal Engineering Conference, ASCE. pp. 526–539.

Rey, V., Belzons, M., Guazzelli, E., 1992. Propagation of surface gravity waves over a rectangular submerged bar. Journal of Fluid Mechanics 235, 453–479.

Saad, Y., Schultz, M. H., 1986. GMRES: A generalized minimum residual algorithm for solving nonsymmetric linear systems. SIAM Journal of Statistical and Scientific Computing 7 (3), 856–869.

Sommerfeld, A., 1949. Partial Differential Equations in Physics. Academic Press, New York.

Takano, K., 1960. Effets d'un obstacle parallélépipédique sur la propagation de la houle. La Houille Blanche 3 (2), 247–267.

Trefethen, L. N., Bau III, D., 1997. Numerical Linear Algebra. SIAM, Philadelphia.

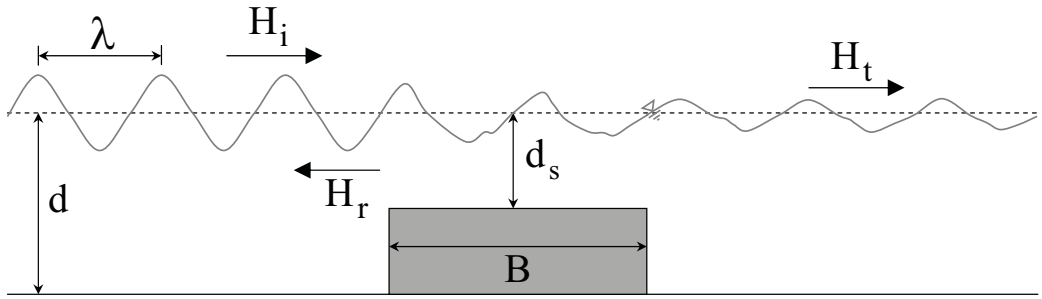

Fig. 1. Schematic indicating notations.

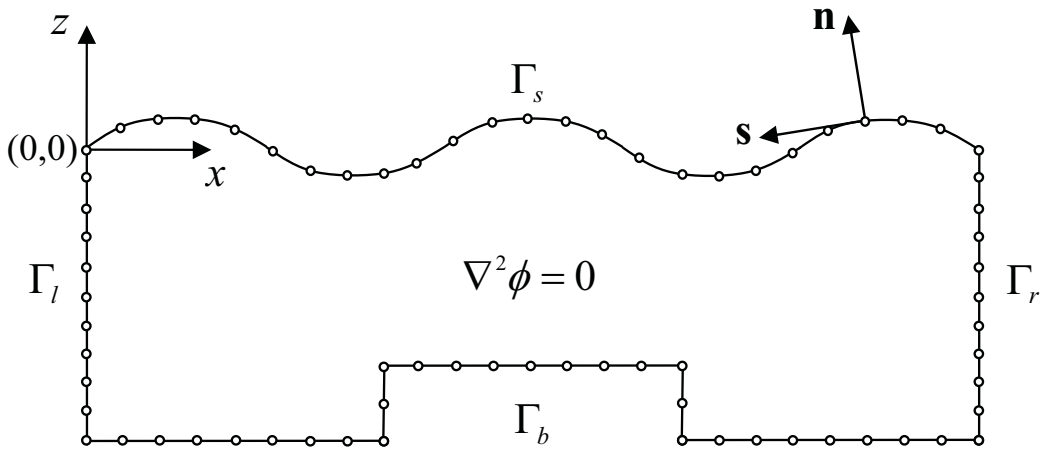

Fig. 2. Schematic of the BEM domain.

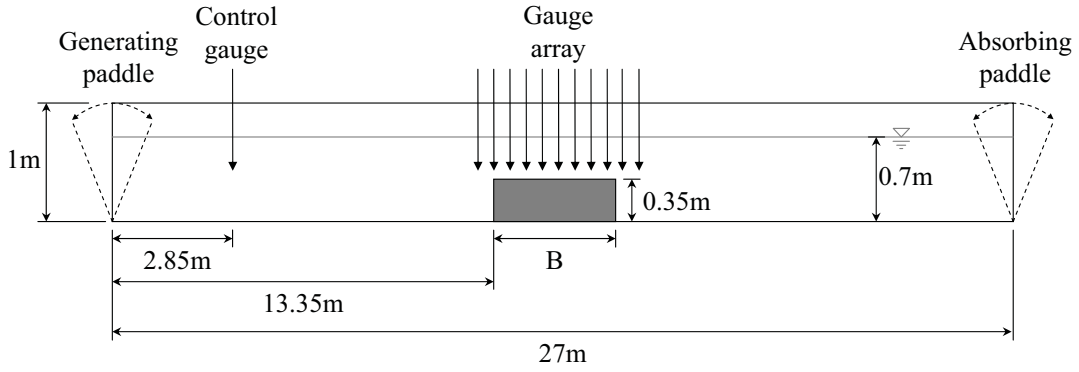

Fig. 3. A sketch showing the layout of the wave flume (not to scale).

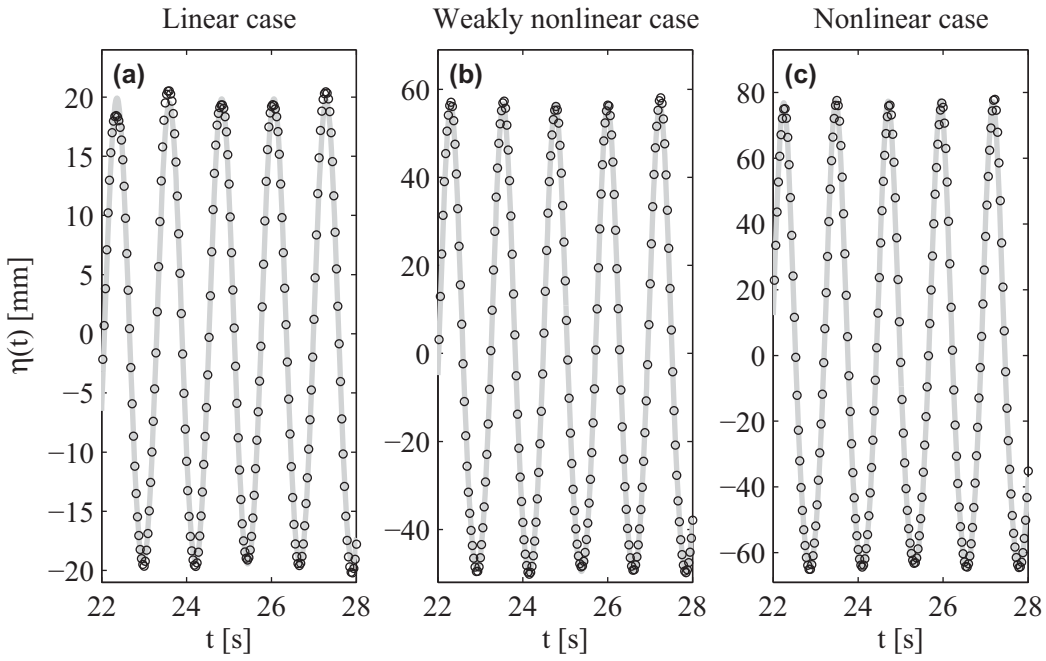

Fig. 4. Incident water surface elevations, $\eta(t)$, 13.95m downstream of the generating wave paddle produced in the absence of the submerged breakwaters: (a) linear, (b) weakly nonlinear and (c) nonlinear wave cases. o Experimental observations, —— BEM.

Table 1

Regular wave cases.

Case	H [mm]	k [rad/m]	$Hk/2$ [-]	λ [m]	d [m]
Linear	39.2	2.769	0.054	2.269	0.7
Weakly nonlinear	106.2	2.769	0.147	2.269	0.7
Nonlinear	142.1	2.769	0.197	2.269	0.7

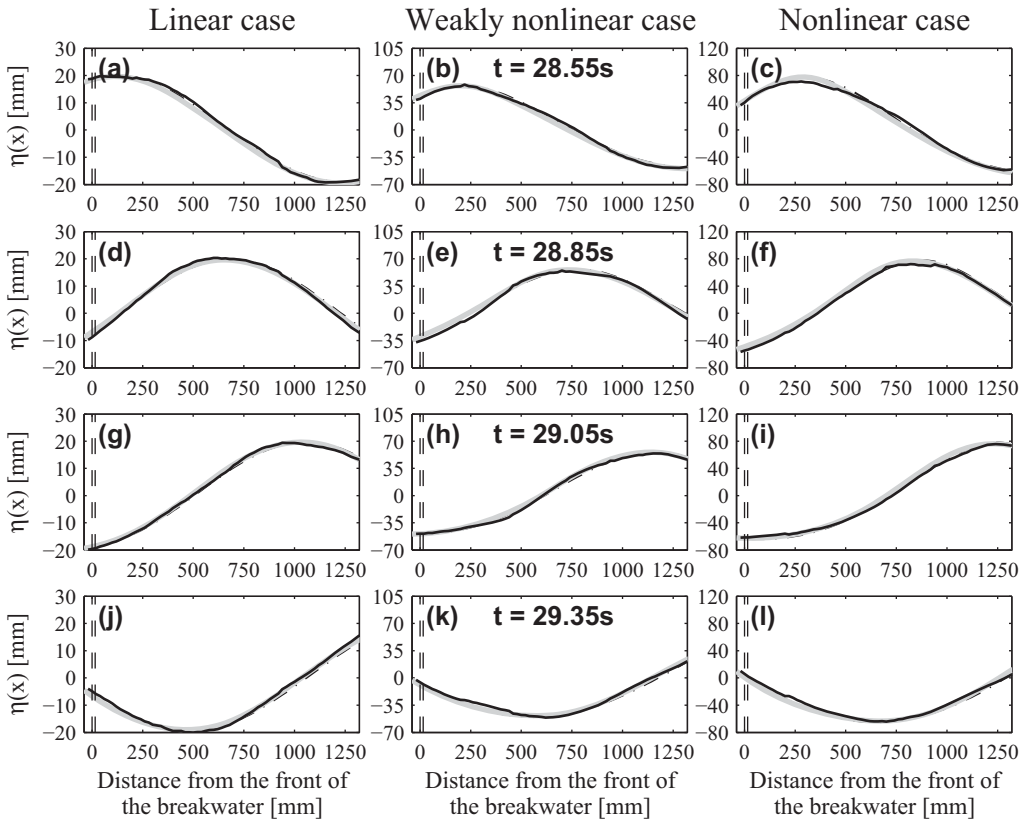

Fig. 5. The spatial surface elevation, $\eta(x)$, in the vicinity of a submerged breakwater of crest width $B = 1.5$cm. —— Experimental observations, - · - · - BEM predictions without a structure, —— BEM predictions with a structure. (Note: the dashed lines indicate the extent of the breakwater).

Table 2

Number of elements and typical run times for each computational domain.

B [cm]	N_E [-]	**Run time per step** [s]
1.5	406	1.28
35.0	396	1.22
70.0	398	1.23
105.0	410	1.30

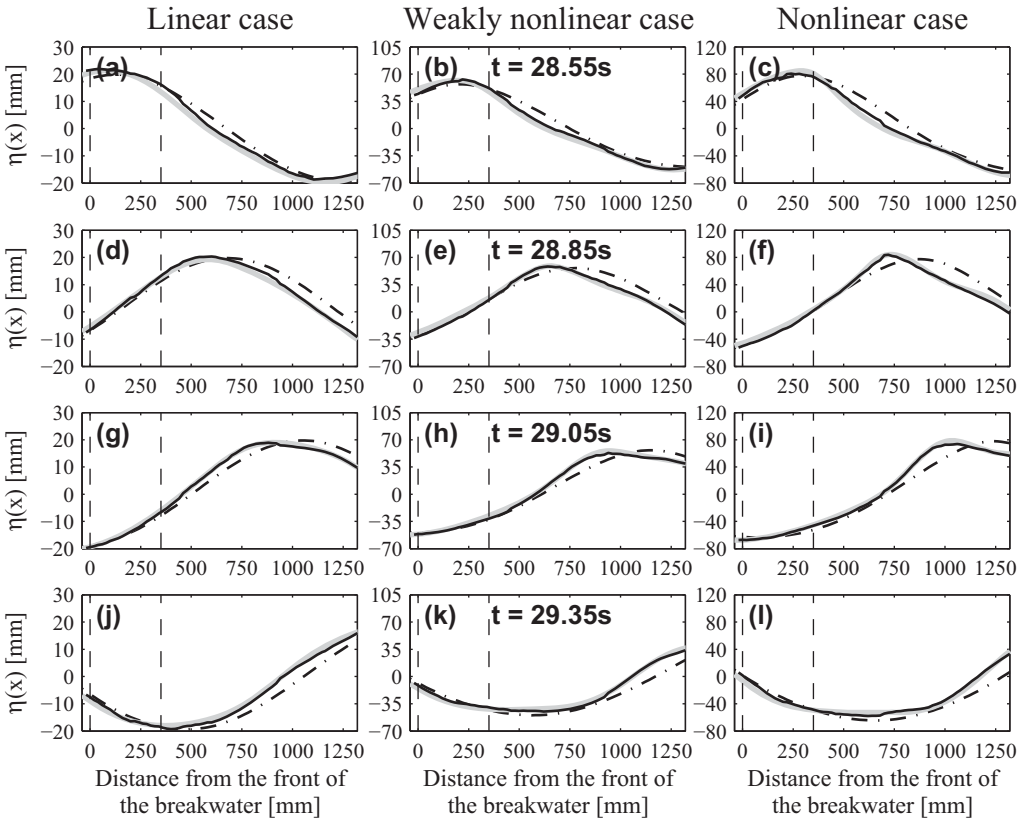

Fig. 6. The spatial surface elevation, $\eta(x)$, in the vicinity of a submerged breakwater of crest width $B = 35$cm. —— Experimental observations, - · - · - BEM predictions without a structure, —— BEM predictions with a structure. (Note: the dashed lines indicate the extent of the breakwater).

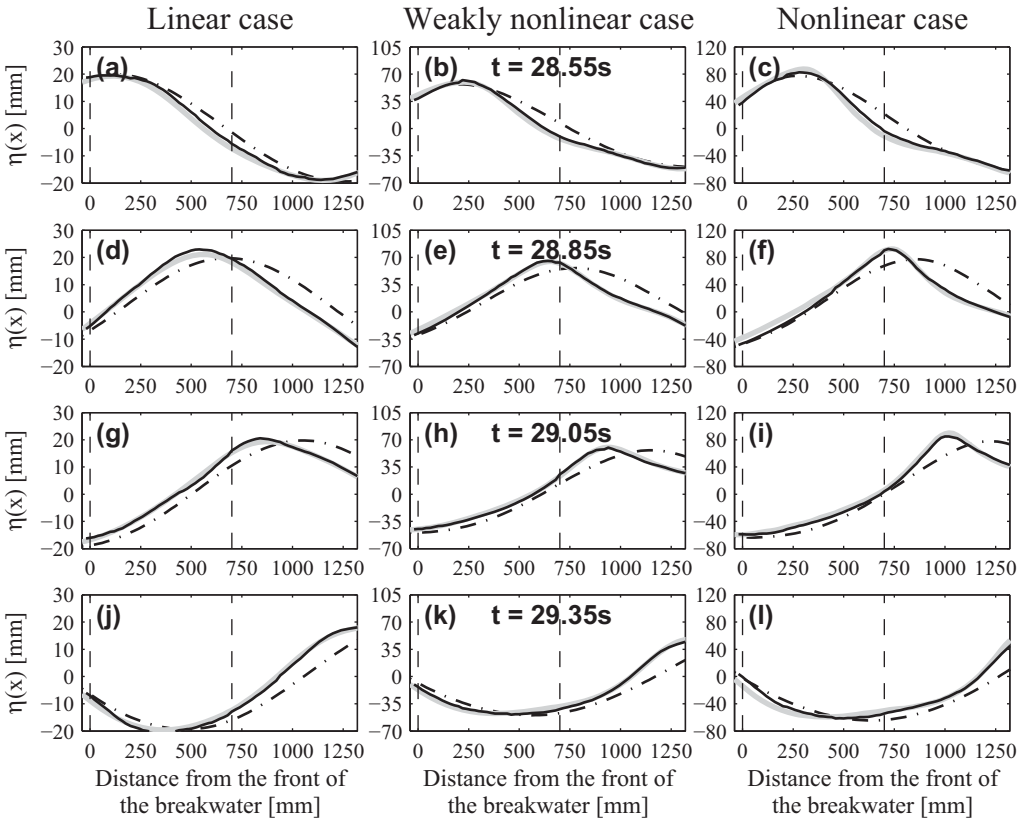

Fig. 7. The spatial surface elevation, $\eta(x)$, in the vicinity of a submerged breakwater of crest width $B = 70$cm. —— Experimental observations, - · - · - BEM predictions without a structure, —— BEM predictions with a structure. (Note: the dashed lines indicate the extent of the breakwater).

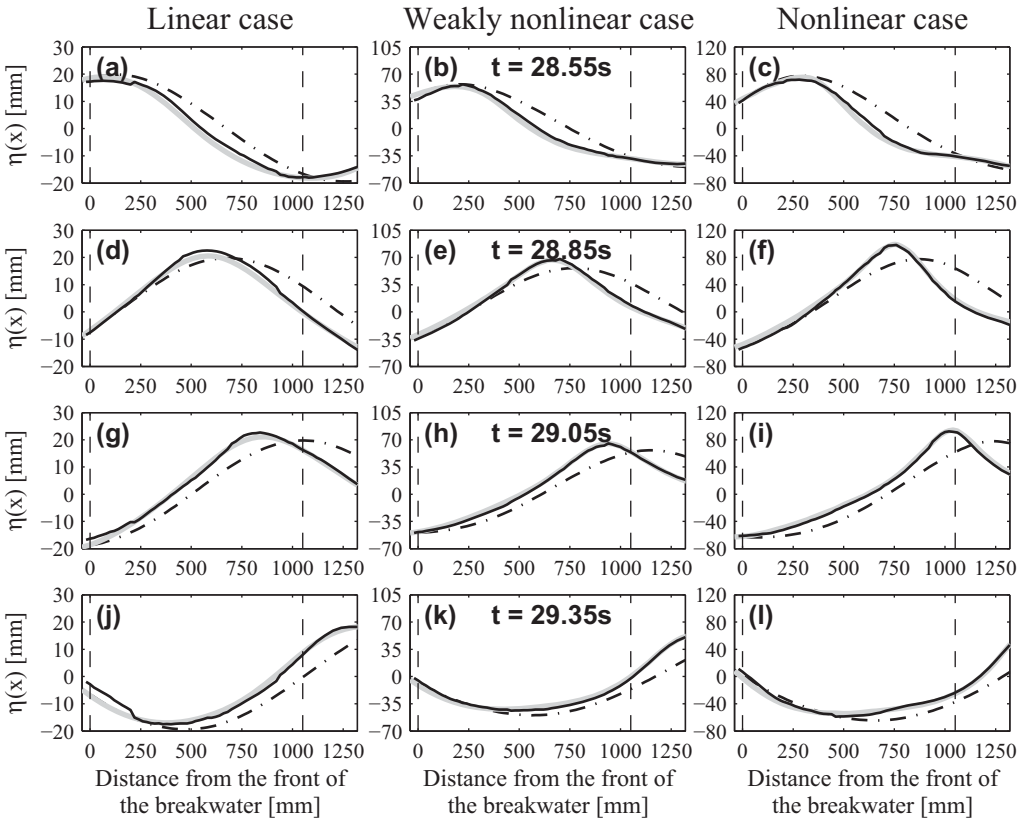

Fig. 8. The spatial surface elevation, $\eta(x)$, in the vicinity of a submerged breakwater of crest width $B = 105$cm. —— Experimental observations, - · - · - BEM predictions without a structure, —— BEM predictions with a structure. (Note: the dashed lines indicate the extent of the breakwater).

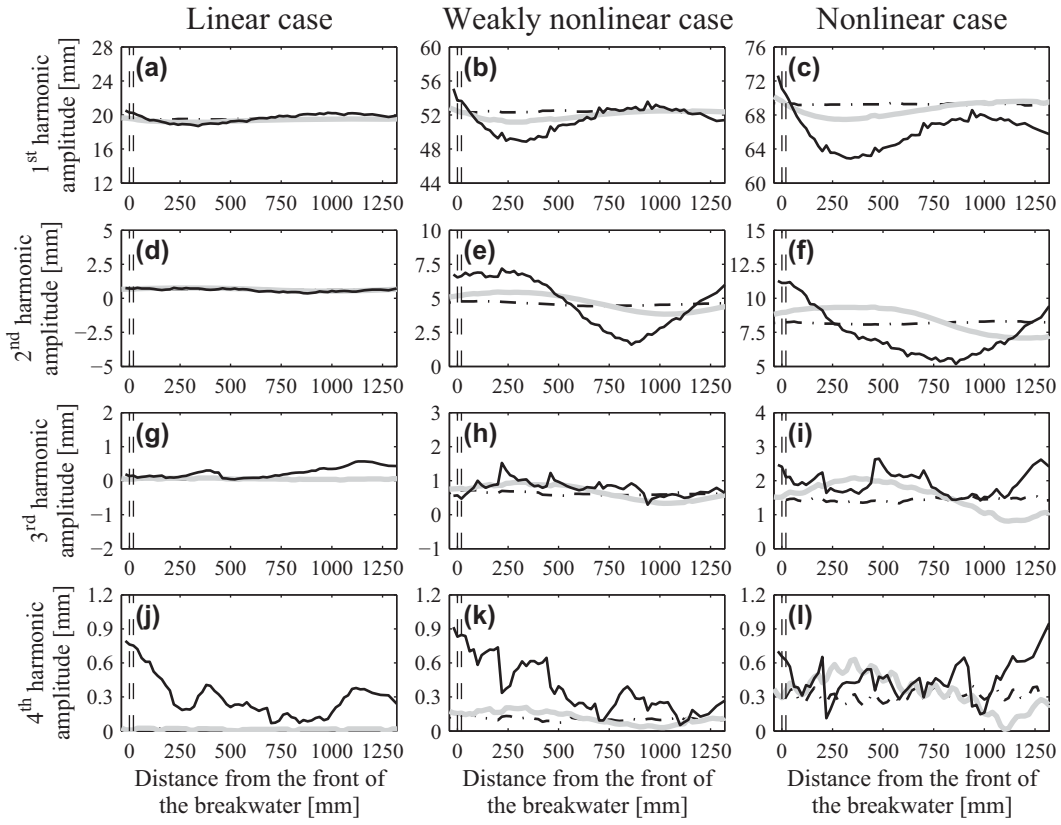

Fig. 9. The harmonic generation produced by a submerged breakwater of crest width $B = 1.5$cm. —— Experimental observations, - · - · - BEM predictions without a structure, —— BEM predictions with a structure. (Note: the dashed lines indicate the extent of the breakwater).

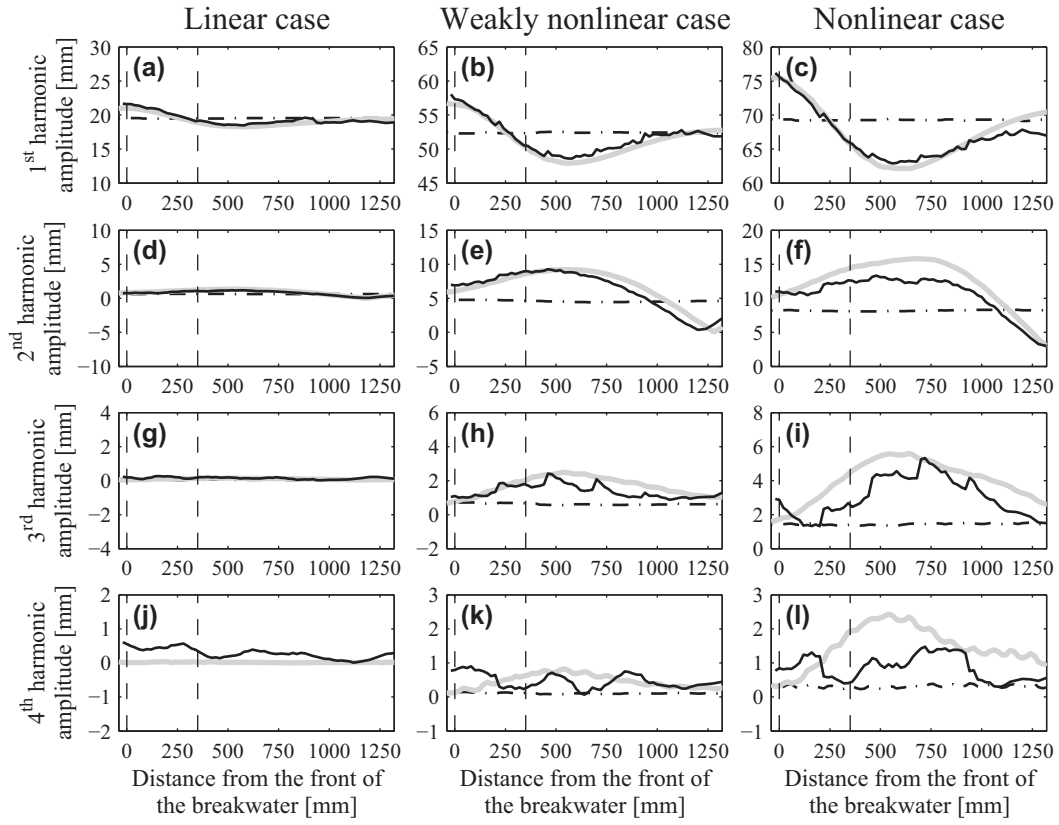

Fig. 10. The harmonic generation produced by a submerged breakwater of crest width $B = 35$cm. —— Experimental observations, - · - · - BEM predictions without a structure, —— BEM predictions with a structure. (Note: the dashed lines indicate the extent of the breakwater).

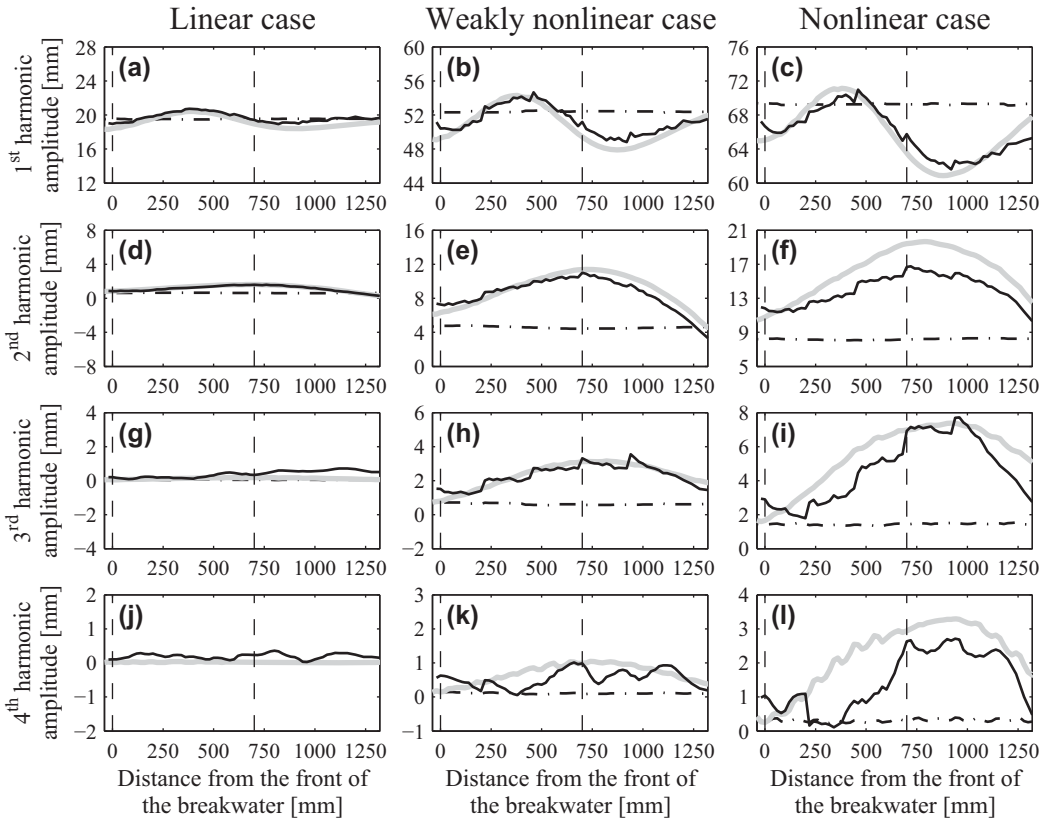

Fig. 11. The harmonic generation produced by a submerged breakwater of crest width $B = 70$cm. —— Experimental observations, - · - · - BEM predictions without a structure, —— BEM predictions with a structure. (Note: the dashed lines indicate the extent of the breakwater).

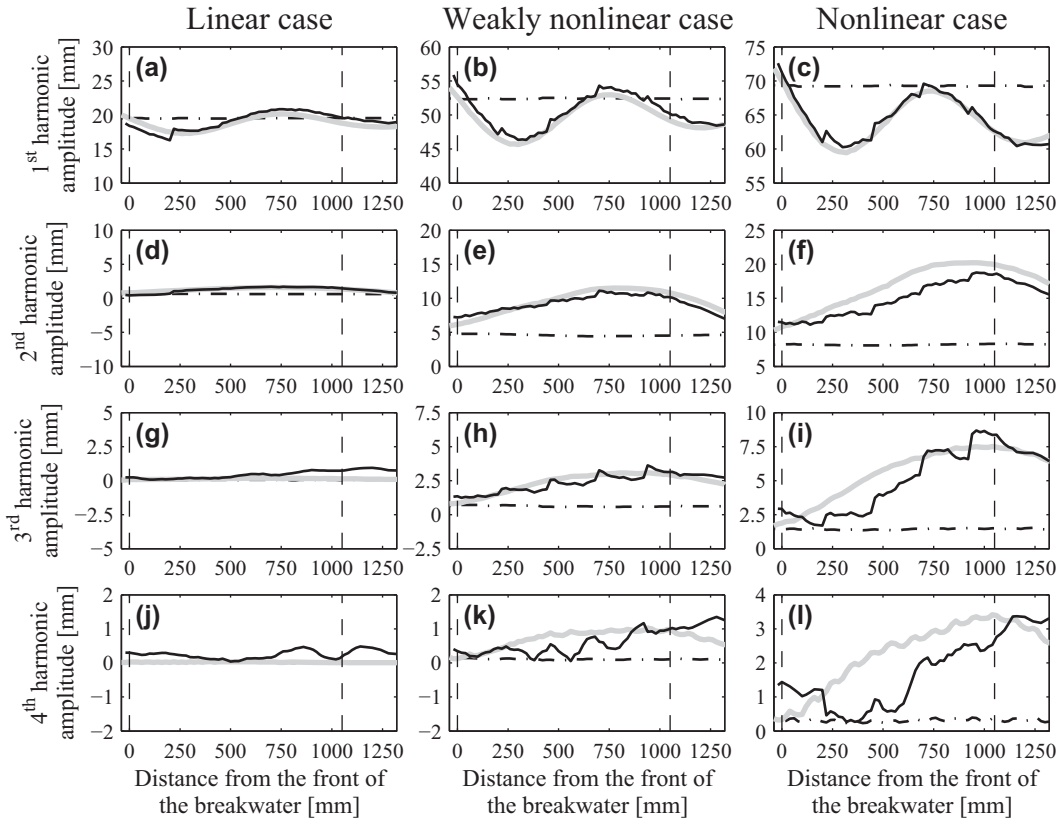

Fig. 12. The harmonic generation produced by a submerged breakwater of crest width $B = 105$cm. —— Experimental observations, - · - · - BEM predictions without a structure, —— BEM predictions with a structure. (Note: the dashed lines indicate the extent of the breakwater).

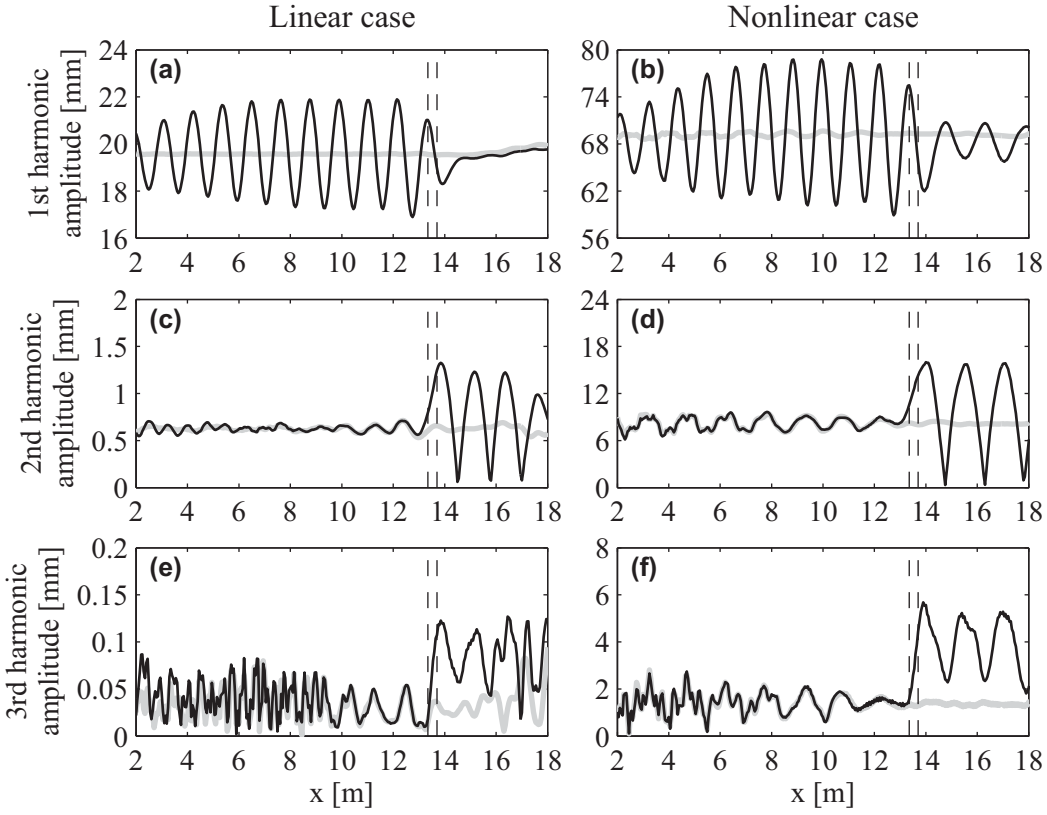

Fig. 13. Harmonic evolution throughout the entire computational domain. ═══ BEM predictions of the incident wave (no structure), ═══ BEM predictions with a submerged breakwater of crest width $B = 35$cm. (Note: the dashed lines indicate the extent of the breakwater).

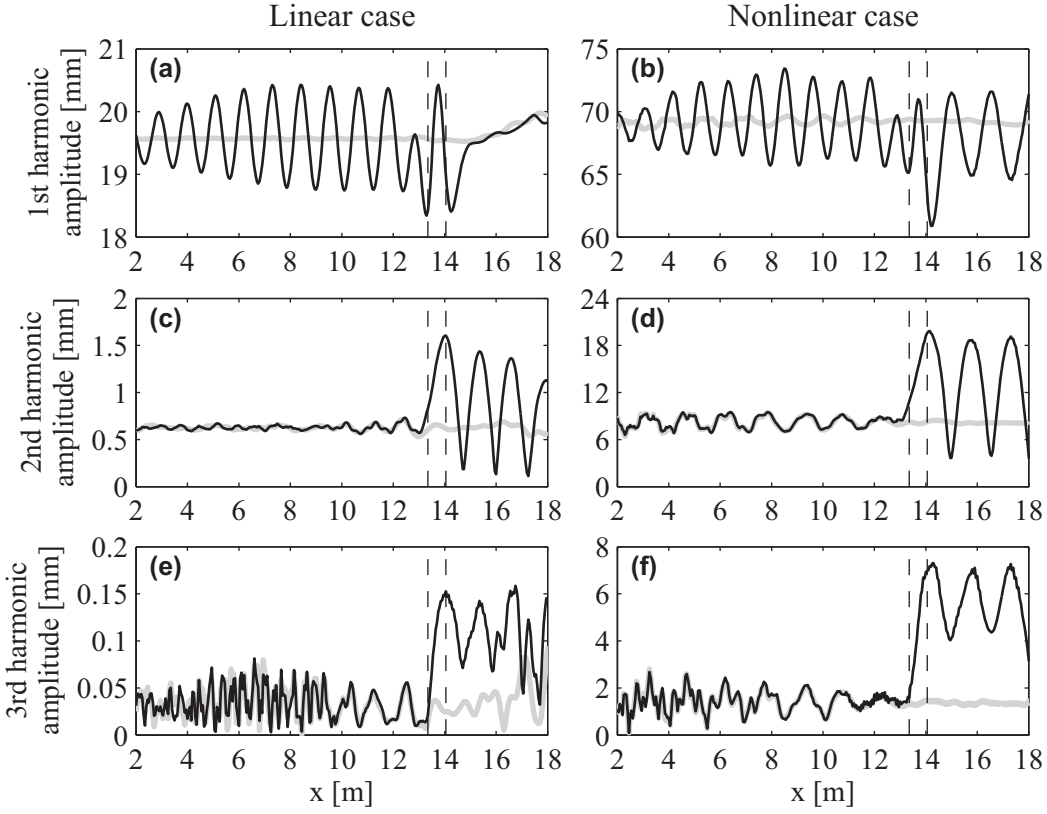

Fig. 14. Harmonic evolution throughout the entire computational domain. ═══ BEM predictions of the incident wave (no structure), ═══ BEM predictions with a submerged breakwater of crest width $B = 70$cm. (Note: the dashed lines indicate the extent of the breakwater).

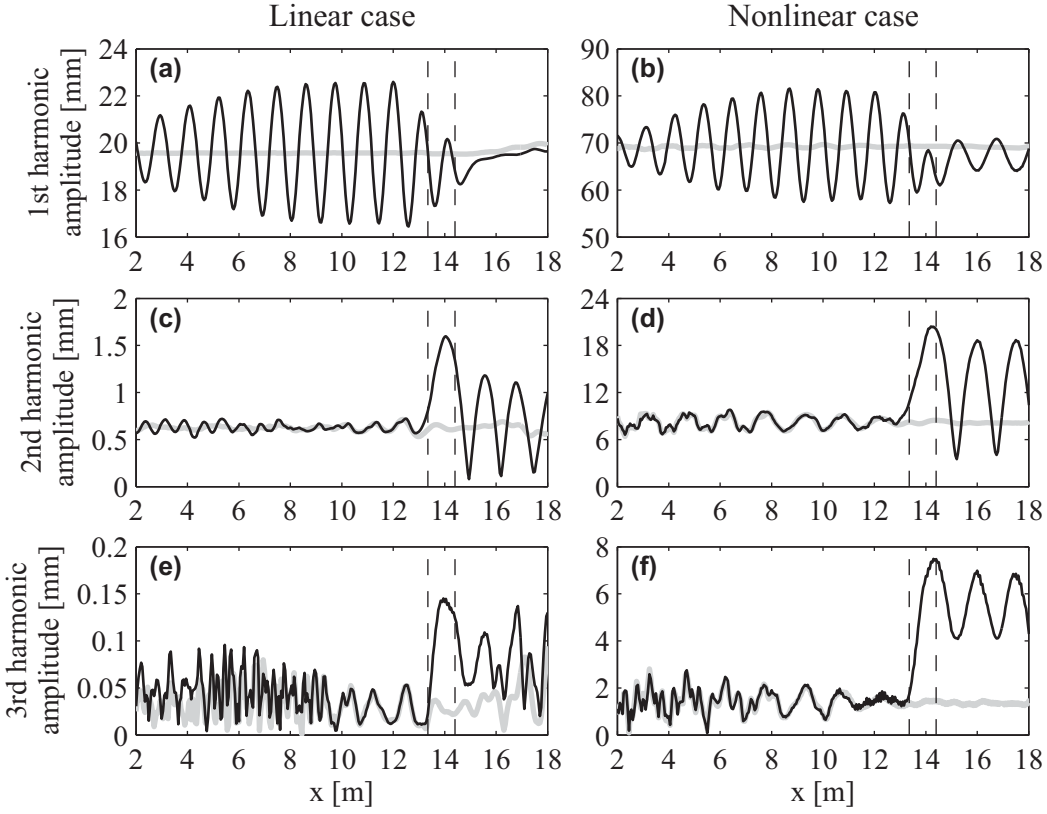

Fig. 15. Harmonic evolution throughout the entire computational domain. ═══ BEM predictions of the incident wave (no structure), ═══ BEM predictions with a submerged breakwater of crest width $B = 105$cm. (Note: the dashed lines indicate the extent of the breakwater).

Table 3

Oscillation beat lengths calculated by the BEM model for the three wave cases and different breakwater crest widths (Note: the superscript of L_t indicates the harmonic involved).

Case	**Linear**			**Weakly nonlinear**			**Nonlinear**		
B [cm]	**35**	**70**	**105**	**35**	**70**	**105**	**35**	**70**	**105**
$\mathbf{L_t^{(1)}}$ [m]	-	-	-	1.350	1.400	1.450	1.550	1.550	1.500
$\mathbf{L_t^{(2)}}$ [m]	1.217	1.225	1.225	1.375	1.375	1.375	1.525	1.550	1.550
$\mathbf{L_t^{(3)}}$ [m]	-	-	-	1.400	1.350	1.350	1.525	1.525	1.500